Preprint Title Ultrafast signatures of magnetic inhomogeneity in $Pd_{1-x}Fe_x$ ($x \leq 0.08$) epitaxial thin films

Authors Andrey V. Petrov, Sergey I. Nikitin, Lenar R. Tagirov, Amir I. Gumarov, Igor V. Yanilkin and Roman V. Yusupov

Publication Date 05 Apr. 2022

Article Type Full Research Paper

ORCID® iDs Andrey V. Petrov - https://orcid.org/0000-0003-3202-2477; Amir I. Gumarov - https://orcid.org/0000-0002-7250-4377; Igor V. Yanilkin - https://orcid.org/0000-0002-8879-8904; Roman V. Yusupov - https://orcid.org/0000-0002-7516-2392

Ultrafast signatures of magnetic inhomogeneity in $Pd_{1-x}Fe_x$ ($x \leq 0.08$) epitaxial thin films

Petrov A.V.[1], Nikitin S.I.[1], Tagirov L.R.[2], Gumarov A.I.[1,2], Yanilkin I.V.[1], and Yusupov R.V.[1]

[1] *Kazan Federal University, Kremlyovskaya 18, Kazan, Russia*

[2] *Zavoisky Kazan Physical-Technical Institute, Sibirsky trakt 10/7, Kazan, Russia*

[*]Correspondence: Roman.Yusupov@kpfu.ru

Abstract. A series of $Pd_{1-x}Fe_x$ alloy epitaxial films (x = 0, 0.038, 0.062, and 0.080), a material promising for superconducting spintronics, was prepared and studied with ultrafast optical and magnetooptical laser spectroscopies in a wide 4 – 300 K temperature range. It was found that the transition to the ferromagnetic state causes the qualitative modification of both the reflectivity and the magnetooptical Kerr effect transients. Nanoscale magnetic inhomogeneity of the ferromagnet/paramagnet type inherent in the palladium-rich $Pd_{1-x}Fe_x$ alloys reveals itself in an occurrence of a relatively slow, 10-25 ps, photoinduced demagnetization component following a subpicosecond one; the former vanishes at low temperatures only in the x = 0.080 sample. We argue that the 10-ps timescale demagnetization originates most probably from the *d*-electron diffusive transport in the conditions of the nanometer-scale magnetic inhomogeneity. The low-temperature amount of the residual paramagnetic phase can be deduced from the magnitude of the slow reflectivity relaxation component, and is estimated as ~ 30% for x = 0.038 and ~ 15% for x = 0.062 films. The minimal iron content ensuring the magnetic homogeneity of the ferromagnetic state in $Pd_{1-x}Fe_x$ alloy at low temperatures is about 7–8 at.%.

Keywords:

Pd-Fe alloy, thin epitaxial film, time-resolved optical spectroscopy, time-resolved magneto-optical Kerr effect, magnetic inhomogeneities

Introduction

Superconducting spintronics is one of the technologies promising for exaflop-scale supercomputing, big-data processing, and artificial intelligence [1-5]. The highlighting features of the superconducting spintronic systems, for example, RSFQ-logic [1-7], are the high speed and unprecedental energy efficiency [2,3,8-11]. The important components here are thin-film magnetic Josephson junctions (MJJ), which include layers of superconductors (S) and ferromagnets (F) [1-3]. The phase difference of the superconducting wave function between S-layers in the three-layer S/F/S structures (or, more practical, SIsFS structures [12,13], where I is an insulator, and s is a superconducting interlayer) is determined by the thickness and the exchange splitting of the conduction band of the F-material. The use of MJJ considerably reduces the number of Josephson junctions and interconnects in the superconducting digital circuitries [14] ensuring wide operation margin tolerances and low bit-error rates [15,16].

To realize the full functionality of superconducting digital circuits, several kinds of MJJ devices are required including logic gates [17-21], programmable logics [14], non-dissipative

biasing [1], random access and cache memories [15,22-26] etc. From the fabrication point of view, it is strongly desirable to utilize a universal tunable ferromagnetic material for every application. Among several candidates [1-3], the palladium-rich $Pd_{1-x}Fe_x$ alloy looks attractive because of the noble-metal base robust against deterioration and the possibility to tune the magnetic properties of $Pd_{1-x}Fe_x$ alloy film by varying the iron content x and preparation conditions [27,28]. Moreover, attempts have been made to use this material (with low, x = 0.01-0.03, iron concentrations) for MJJ memory applications [1,12,13,22,29,30]. However, these studies faced the problems of small critical current and temporal instability of magnetic properties [31]. On one hand, nanoscale magnetic inhomogeneities are inherent in disordered $Pd_{1-x}Fe_x$ alloys with a high palladium content, on the other hand, they are extremely undesirable when used in MJJ. Indeed, within the frames of the percolation model of ferromagnetism in the $Pd_{1-x}Fe_x$ alloy at x <0.1 [32,33], magnetic inhomogeneities cause spin-flip and the pairing wave function damping, hence, reducing the Josephson critical current magnitude. Small-scale inhomogeneities are difficult to detect with either conventional neutron-scattering methods (see review [32] and references therein) or with the stationary magneto-optical Kerr/Faraday effects and ~~or~~ ferromagnetic resonance techniques (the latter two – because of the large scale, volume-averaged signals). Resonant magnetic small-angle x-ray scattering (RMSAXS) applied to $Pd_{1-x}Fe_x$ alloy film at x = 0.03-0.07 revealed static magnetic fluctuations on the lateral scale of about 100 nm attributed to the magnetic domain structures of the films [34]. Smaller-scale fluctuations due to intrinsic disorder in the alloy composition still remain unexplored.

Finding a way to achieve magnetic uniformity in $Pd_{1-x}Fe_x$ down to atomic scale is a challenge. One of the options is the selection of the concentration range of iron, at which the alloy would become magnetically homogeneous. This requires a method for detecting magnetic inhomogeneities, preferably with the possibility of being applied to thin films. We propose the use of ultrafast, time-resolved optical and magneto-optical spectroscopy methods for probing magnetic inhomogeneities in thin films: individual constituents can be characterized by specific relaxation components that can be used to detect magnetic inhomogeneities and track their evolutions. In addition, the peculiarities of the magnetization dynamics in magnetically inhomogeneous systems are of the interest themselves.

In our recent work, using the example of a thin epitaxial film of $Pd_{0.94}Fe_{0.06}$, it was demonstrated [35] that the dynamics of the reflection coefficient and the angle of rotation of the polarization plane in the magneto-optical Kerr effect (MOKE) after a photoexcitation with femtosecond light pulses contain the components whose temperature dependence correlates with that of the spontaneous magnetization. It was argued that such responses can serve as a source of

information on magnetic inhomogeneity. In this work, we extend the series of $Pd_{1-x}Fe_x$ films to a wider concentration range, confirm the correlation of the ultrafast responses with the magnetic properties of the system, and determine the minimum iron concentration in the alloy that ensures its magnetic homogeneity at low temperatures. We discuss the findings in the frame of a model in which ferromagnetic (FM) and paramagnetic (PM) regions coexist, with the latter collapsing upon an increase of the iron content.

Samples and experimental techniques

The samples for the studies were thin epitaxial films of $Pd_{1-x}Fe_x$ with the nominal content of the iron $x = 0$ (pure Pd), 0.038, 0.062, and 0.080 grown on the single-crystal MgO (001) substrates by molecular beam epitaxy. The films were 20 nm thick, continuous and smooth monocrystalline layers. Details of the synthesis and characterization of the samples used in the work can be found in our previous papers [27,28]. The Curie temperatures for the samples with $x = 0.038$, 0.062, and 0.080 were ~ 120 K, ~ 177 K, and ~ 210 K, respectively.

The optical experiments were carried out in a pump-probe arrangement with the *Legend-USP* regenerative amplifier from *COHERENT* used as a light sourse. The pulse repetition rate was 970 Hz, central wavelength 800 nm, and the duration – 40 fs. Excitation of the samples was performed by the pump light with a wavelength of 400 nm (second harmonic) and probing of their properties – at 800 nm. The pump and probe beams were focused at the sample into the spots with the diameters of 0.5 mm and 0.1 mm, respectively. Energy densities of the pump and the probe were 1 mJ/cm^2 and 50 μJ/cm^2, and incidence angles were ~ 2 and ~ 18 degrees.

The relaxation of the electronic subsystem was monitored by the relative change in the reflection coefficient ($\Delta R/R$). Ultrafast dynamics of the magnetization was analyzed by the deviation of the angle of rotation of the polarization plane of the probing light from the equilibrium in the longitudinal magneto-optical Kerr effect (MOKE). The probing light reflected from the sample passed through a Wollaston prism dividing the beam into two orthogonally polarized components. The intensities of these two components were detected by *Hamamatsu S2386-5K* silicon photodiodes. The difference signal from the output of the photodiodes was used to determine the Kerr rotation angle, and the sum signal was used to measure the dynamics of the reflection coefficient. To extract the magnetic contribution to the rotation of the polarization plane, which partially can originate from the pump-induced anisotropy, the responses were measured at two oppositely applied magnetic fields. In this case, the contribution odd with respect to the sign of the field has a magnetic nature.

To perform measurements at temperatures from 4.2 to 300 K, the films under study were mounted to the cold finger of the *Janis ST-500* helium-flow cryostat. Permanent NdFeB magnets were fixed there, creating a magnetic field directed along the easy axis of the thin film in its plane with a magnitude of 470 Oe at room temperature. This field strength ensures a uniformly magnetized state of the film since the coercive field of the studied samples does not exceed 25 Oe. The sample temperature was set and maintained using the Lakeshore 335 temperature controller with an accuracy of 0.1 K.

Results

Figure 1 shows the dependences of the reflectivity normalized to the equilibrium value on the delay between the pump and the probe pulses of the four studied samples and their variations with temperature in the range of 5 – 300 K. In general, the responses of the pure palladium film change very slightly with temperature. The addition of the iron dopant leads to a development of a temperature dependence of $\Delta R/R(\Delta t)$ responses, both qualitative (the appearance of new relaxation components) and quantitative (changes in their amplitudes and time constants). While two decaying exponents are sufficient to describe the relaxation of the reflection coefficient of the Pd and $Pd_{0.962}Fe_{0.038}$ films at the lowest temperature, a minimum of four is required for the $Pd_{0.94}Fe_{0.06}$ film and only three for $Pd_{0.92}Fe_{0.08}$. Thus, with an increase in the iron concentration x in a $Pd_{1-x}Fe_x$ system, the photoinduced dynamics of the electronic subsystem changes from a relatively simple to a much more complex one; then, the character partially simplifies.

In quantitative terms, in the general case, the relaxation response can be described by the sum of four decaying exponents – two fast and two relatively slow ones, with one positive and one negative amplitude in each pair:

$$-\Delta R / R(\Delta t) = A_f e^{-\Delta t/\tau_f^A} + A_s e^{-\Delta t/\tau_s^A} - B_f e^{-\Delta t/\tau_f^B} - B_s e^{-\Delta t/\tau_s^B}. \quad (1)$$

A significant difference in the values of the characteristic times for the fast and slow components makes it possible to fit them separately, which improves the accuracy of the parameter determination.

To describe the relaxation of the reflectivity of a palladium film, Figure 1a, the first two terms in Equation (1) are sufficient. The fast component with an amplitude A_f has a decay time $\tau_f^A = 0.24 \pm 0.02$ ps. The lifetime of the second – slow – component with the amplitude A_s is $\tau_s^A = 410 \pm 10$ ps. Panels (b)-(d) in Figure 1 show similar dynamics of the reflectance for three films with iron contents of 3.8, 6.2 and 8.0 at.%. At room temperature, the behavior of the responses for the films with 3.8 and 6.2 at.% of iron is similar to the responses obtained from the

pure Pd film. The above-mentioned fast component for these films has approximately the same lifetime ~ 0.3 ps. The lifetime of the slow component in the samples with 3.8, 6.2, and 8.0 at.% of iron is 240 ± 10 ps, 210 ± 10 ps, 290 ± 10 ps, respectively. However, with an increase in the iron concentration, at times up to ~ 10 ps, an additional fast exponential decaying component appears. This component is opposite in sign to those given above. The main feature of these responses is their strong temperature dependence. At temperatures above the Curie temperature of the samples, they are not detectable. However, on cooling, starting from the Curie temperature, $\Delta R/R(\Delta t)$ responses sharply. The amplitude of the fast negative component increases in absolute value. Also, both the amplitude and the relaxation time of the slow positive component decrease. At temperatures of 90 K and 160 K, another slow negative component appears in the samples with 6 and 8 at.% of iron, respectively. Its relaxation time is about 1 ns. The amplitude of this component is an order of magnitude smaller than the amplitudes of the other components.

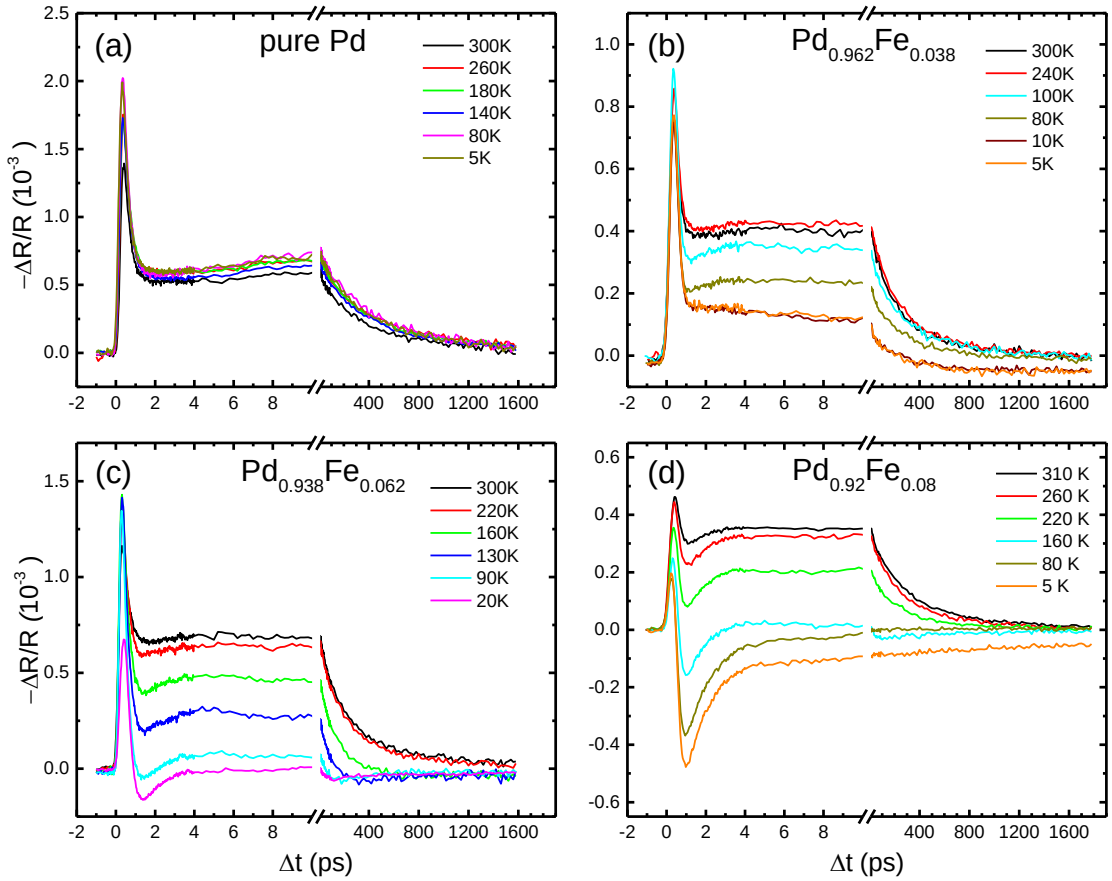

Figure 1. Temperature evolutions of the reflectivity transients of $Pd_{1-x}Fe_x$ alloy thin epitaxial films for compositions with x = 0 (a), 0.038 (b), 0.062 (c), and 0.080 (d).

Figure 2 shows temperature dependences of the ultrafast dynamics of magnetization. The data are presented here for the films with x = 0.038 and x = 0.080; for the sample with x = 0.062,

the responses can be found in [35]. Photoinduced demagnetization and the recovery are observed only at $T < T_C$. In the figure, one can readily recognize two demagnetization processes that reveal themselves as the rising components and occur at a subpicosecond and ~ 10 ps time scales. Therefore, the responses in the general case are described by the expression:

$$\Delta\theta_K(\Delta t) = \left[A_{r1}^K \left(1 - e^{-\Delta t/\tau_{r1}^K}\right) + A_{r2}^K \left(1 - e^{-\Delta t/\tau_{r2}^K}\right) \right] \times e^{-\Delta t/\tau_d^K}, \quad (2)$$

where components with amplitudes A_{r1}^K and A_{r2}^K describe the rise (demagnetization), while the factor following the square brackets – the decay of the signal (magnetization recovery).

Temperature dependences of the amplitudes and the lifetimes of the selected components, obtained from the fitting of the experimental data with Eqs. (1) and (2), are presented in Figures 3 and 4 for the reflectivity and TR-MOKE, respectively. We note here the invariance of the amplitude A_s (Fig. 3, a) and relaxation time τ_s^A (Fig. 3, b) at $T \geq T_C$, and a kink in their dependences at $T = T_C$ for the films with x = 0.038 and 0.062. The evolution of this component is not so obvious for the film with x = 0.080: the kink in its temperature dependence and the onset of its suppression take place at a temperature slightly above the T_C. Below the T_C, all three samples reveal a decrease of A_s and a shortening of τ_s^A. In the samples with 3.8 at.% and 6.2 at.% of iron, the drop of A_s with the temperature decrease slows down and ceases reaching at 5 K the values of ~ 15% and ~ 30% of its maximum, respectively.

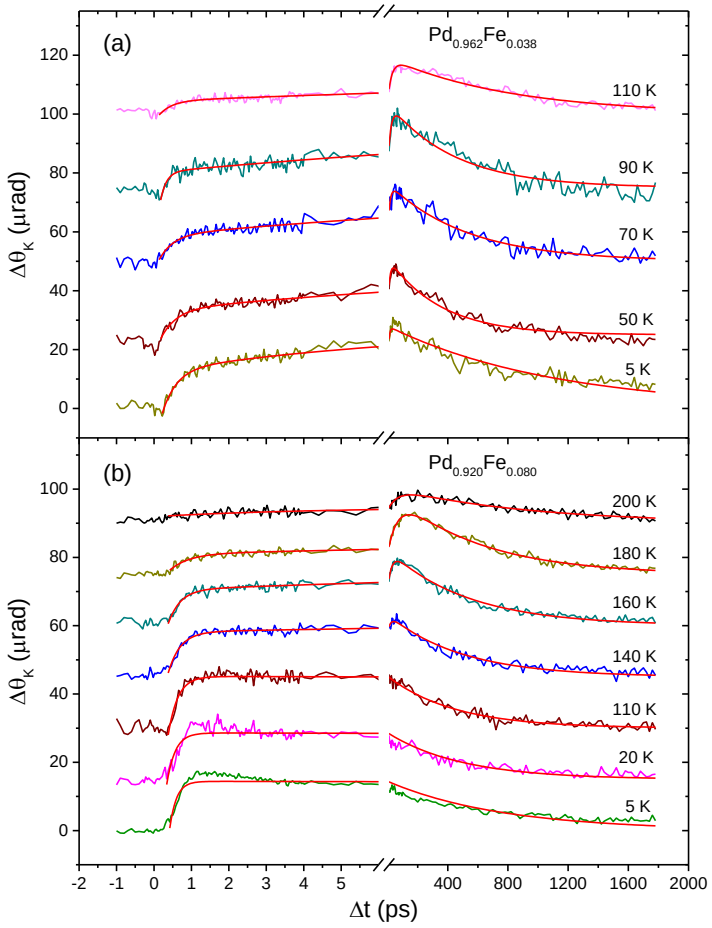

Figure 2. Temperature evolutions of the time-resolved magneto-optic Kerr angle transients for the $Pd_{0.962}Fe_{0.038}$ (a) and $Pd_{0.92}Fe_{0.08}$ (b) epitaxial thin films at $T < T_C$; red solid lines are the results of the fits with Eq. (2).

Other characteristics: amplitudes A_f and B_s, relaxation times τ_f^A and τ_s^B do not reveal any anomalies in their temperature dependences and therefore are not presented. The amplitude of the fast component B_f for each $Pd_{1-x}Fe_x$ alloy film has a nonzero value practically in the entire temperature range of 5 – 300 K. It gradually increases with decreasing temperature for samples with 6.2 and 8.0 at.% of iron. For the sample with 3.8 at.% of iron, it has the same behavior down to 150 K, and then decreases to zero at the lowest temperatures. The relaxation time of this component is practically independent of temperature and is $\tau_f^B = 0.80 \pm 0.10$ ps.

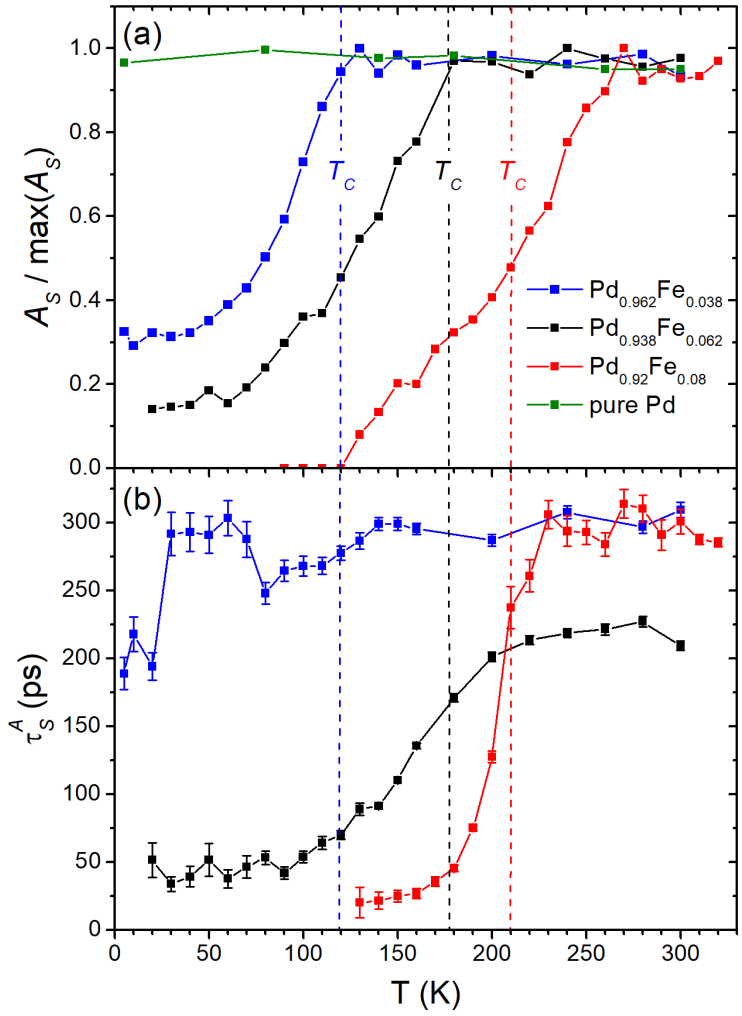

Figure 3. Temperature dependences of the amplitudes (a) and the lifetimes (b) of the slow relaxation components of the reflectivity transients shown in Figure 1. In panel (a) the amplitude A_s for each sample is normalized to its magnitude at room temperature.

Figure 4, a shows the temperature dependences of the amplitudes of the components responsible for the two-component demagnetization process. Here, the fast component is observed in the entire temperature range below the Curie temperatures of the samples. The average rise time of the fast component of demagnetization for all three samples is ~ 0.3 ps and depends only slightly on temperature. The variation with temperature of the amplitude of the slow demagnetization component A_{r2}^K of the $Pd_{0.962}Fe_{0.038}$ sample is similar in character to that of the fast component. In the $Pd_{0.938}Fe_{0.062}$ sample, starting from the T_C, the amplitude A_{r2}^K increases with lowering the temperature and reaches a maximum at ~ 160 K. On further cooling, the amplitude decreases with a tendency to saturate at a small, but still detectable value at the lowest temperatures. In the $Pd_{0.92}Fe_{0.08}$ sample, the slow component is observed only in the range

$120\ \mathrm{K} < T < T_C$. Here, it also appears at the T_C, reaches a maximum at ~ 180 K and drops to zero value at ~125 K.

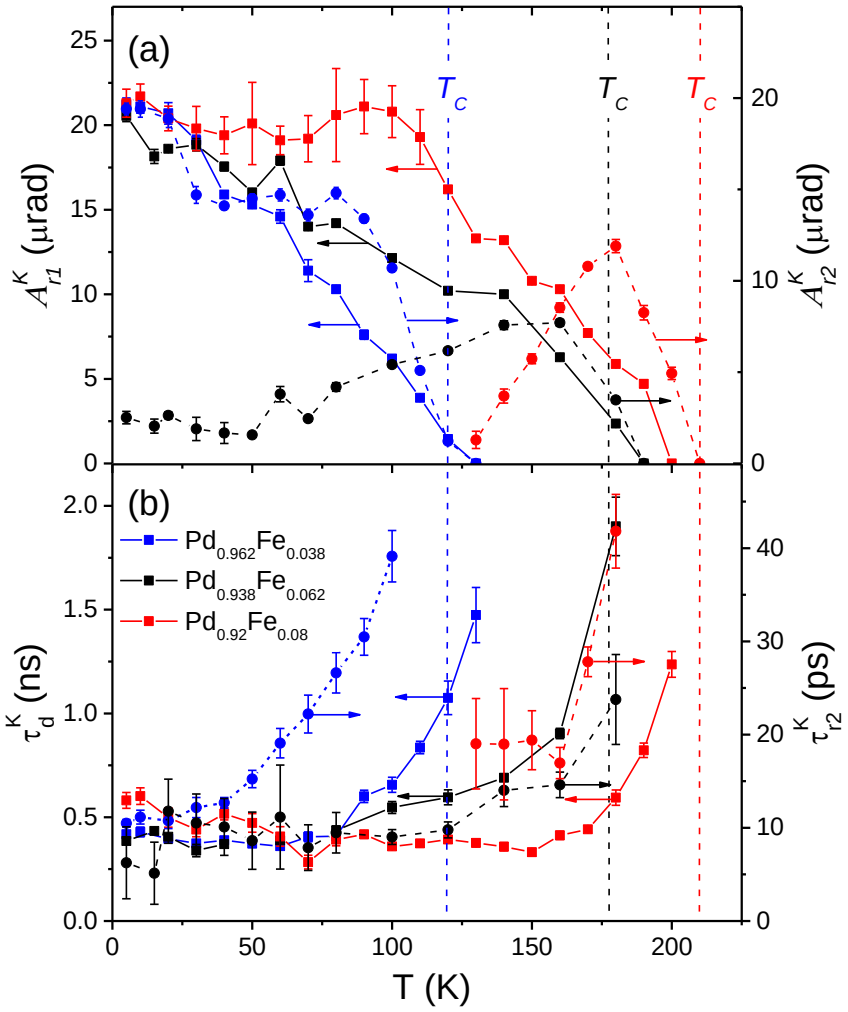

Figure 4. Temperature dependences of the amplitudes (a) of the fast (squares/solid lines) and the slow (circles/dashed lines) photoinduced demagnetization components and characteristic times (b) of the slow demagnetization (circles/dashed lines) and magnetization recovery (squares/solid lines) of the $Pd_{0.962}Fe_{0.038}$ (blue), $Pd_{0.938}Fe_{0.062}$ (black) and $Pd_{0.92}Fe_{0.08}$ (red) epitaxial films.

Temperature dependences of the characteristic time of the slow demagnetization component are shown in Fig. 4, b. It has a minimum value for all films at the lowest temperatures of the range of it's observation. For the samples with an iron content of 3.8 and 6.2 at.%, the minimum τ^K_{r2} is ~ 10 ps, and for a film with 8 at.% of iron, it is ~ 20 ps. However, on warming of a sample, the slow demagnetization time increases and becomes several times longer on approaching the Curie temperature. Magnetization recovery time τ^K_d reveals a similar behavior (Fig. 4, b) demonstrating a kind of a critical slowing down characteristic for second

order phase transitions: starting from a value of ~ 0.5 ns at the lowest temperatures, τ_d^K grows rapidly on approaching the T_C of the samples, where it gets 2-3 times longer.

Discussion of the Results

In this section, we focus our attention at the components of the ultrafast responses of the electronic (reflectivity) and magnetic (Kerr rotation angle) subsystems, which demonstrate a clear correlation with the establishment of the long-range magnetic order in $Pd_{1-x}Fe_x$ films.

In the $\Delta R/R(\Delta t)$ dependences of the alloys, the slow relaxation component with the amplitude A_s (Figure 3, a) follows this trend. While no temperature variation of the A_s is observed for a pure palladium film, a sharp kink close to the T_c's towards its decrease appears for the other three samples. Moreover, for the $Pd_{0.962}Fe_{0.038}$ film, as well as for the $Pd_{0.938}Fe_{0.062}$ film [35], the shape of the properly normalized $A_s(T)$ dependence practically reproduces that for the saturation magnetization $M_s(T)/M_s(0)$ (Figure 5, a). In our opinion, within the framework of the magnetic polaron model [32,33], such a situation can be associated with a decrease in the volume of the paramagnetic phase due to the growth of magnetic bubbles fraction.

It is worthy to note that the A_s amplitude for the $Pd_{0.92}Fe_{0.08}$ sample vanishes below 120 K. Based on the normalized $A_s(T)$ dependences from Figure 3, a, one can estimate that in the $Pd_{0.962}Fe_{0.038}$ sample, about 30% of the film volume is left in the paramagnetic state at low temperatures; for the $Pd_{0.938}Fe_{0.062}$ sample, the volume fraction of the paramagnetic phase is ~15%. The $Pd_{0.92}Fe_{0.08}$ sample is in a homogeneous ferromagnetic state below 120 K. Thus, we associate the slow relaxation of the reflectivity of the $Pd_{1-x}Fe_x$ films with the presence of a residual paramagnetic phase in the sample. It's manifestation at temperatures corresponding to the ferromagnetic state of the material we relate to the presence of magnetic inhomogeneities. The latter are most likely formed due to the inhomogeneous distribution of the iron impurities in the palladium host.

As for the Kerr rotation angle dynamics (Figure 2), any detected signals are observed only at temperatures below the T_C for the each sample. An interesting feature here is the manifestation of two components in the photoinduced demagnetization – the ultrafast component with a characteristic time of ~ 0.3 ps, and a noticeably slower one, occurring on a scale of ~ 10-20 ps. The ultrafast process manifests itself at all temperatures below the T_C, and its amplitude grows gradually on cooling. The slower demagnetization component reveals specific temperature dependences of the amplitude A_{r2}^K that strongly depends on the composition of the film (see Figure 4, a).

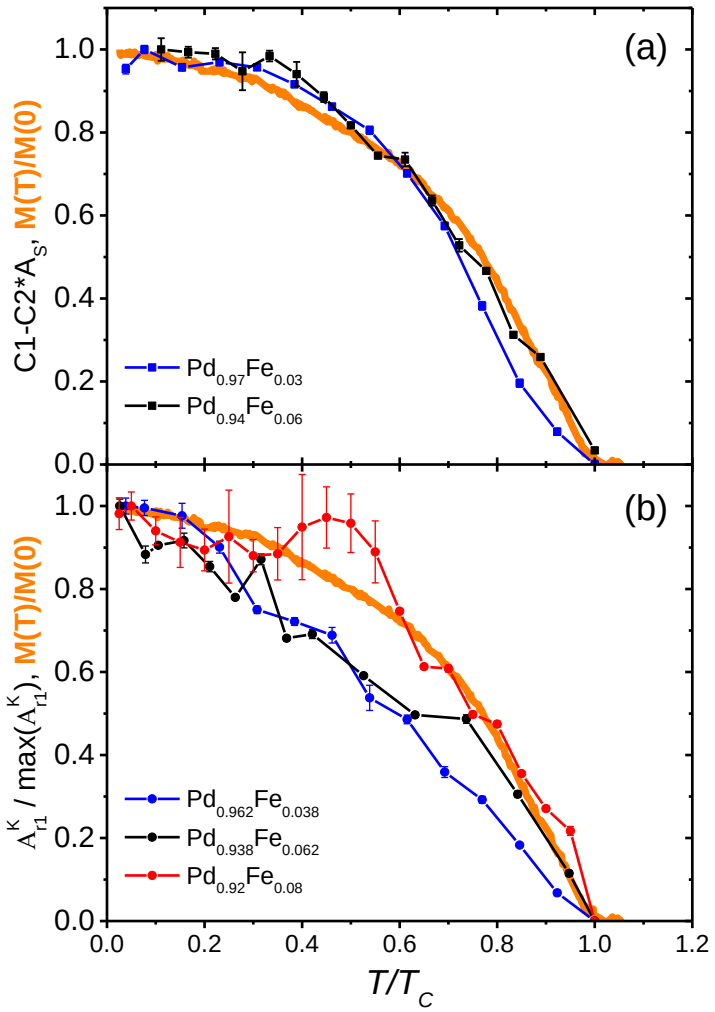

Figure 5. Temperature dependences of the reflectivity slow relaxation amplitudes of the $Pd_{0.962}Fe_{0.038}$ (blue) and $Pd_{0.938}Fe_{0.062}$ (black) samples, transformed and normalized in magnitude for their comparison with the dependence of the saturation magnetization (thick orange line) (a); the same for the Kerr rotation angle dependences (b).

Going deeper into the details, the amplitude A_{r2}^{K} for the sample with $x = 0.03$ increases with decreasing temperature in the entire range of $5\ \mathrm{K} \le T < T_C$. For samples with $x = 0.06$ and 0.08, this amplitude reaches a maximum rather quickly as the temperature drops below T_C, and then behaves differently for these two samples. In the film with $x = 0.06$, this component gradually decreases to a level of 25-30% of the maximum, without turning to zero down to a temperature of 5 K. In the film with $x = 0.08$, on cooling of the sample below the T_C, the amplitude A_{r2}^{K} rapidly decreases after reaching the maximum value. It further approaches zero at 120 K and does not recover at lower temperatures. As we can see from Figures 3, a and 4, a, the observation of the slow component of the demagnetization correlates with the observation of the slow relaxation of the reflectivity (amplitude A_s). In our opinion, this fact makes it possible to relate the slower component of demagnetization with magnetic inhomogeneities in the sample.

The amplitude of this component reaches its maximum, apparently, at temperatures corresponding to the maximum degree of magnetic inhomogeneity of the films. The temperature dependence of the subpicosecond demagnetization component clearly correlates with the course of the saturation magnetization of the film (Figures 4, a and 5, b), and represents thus the response of the ferromagnetic component of the films under study.

Origin of the photoinduced demagnetization components specific for a magnetically inhomogeneous ferromagnetic/paramagnetic metallic state is important itself, therefore should be discussed explicitly. First, we note that $Pd_{1-x}Fe_x$ alloys are systems in which magnetism is mainly due to the polarization of palladium 4*d*-electrons. The second distinguishing feature of $Pd_{1-x}Fe_x$ alloys is their small spatial scale of magnetic inhomogeneities, which is of the order of 1 nm.

The "on-site" photoinduced demagnetization of the FM component of the system, which occurs on a sub-ps time scale, for *d*-electron systems is under intense discussion in past decades [36-41], and we observe the same. In our alloys with the nanoscale magnetic inhomogeneity we detect an additional demagnetization component with unusual characteristic time of ~ 10 ps. Transfer of angular momentum by highly mobile *s*-*p*-electrons (which occurs due to the *s*-*d* interaction [38]) should only increase the rate of photoinduced demagnetization on a sub-ps scale. This mechanism was justified to explain the ultrafast transfer of angular momentum in F/N heterostructures with large (tens of nanometer) layer thicknesses [38,42,43]. However, it cannot explain the additional demagnetization component with a characteristic time of ~10 ps observed in our Pd-Fe alloy system.

It is our hypothesis that spin-diifusion could bring the PM areas into equilibrium with the FM environment and be an origin of the 10 ps transient. Indeed, the diffusion velocity for the ~1 nm size area and the time scale of 10 ps can be estimated as 10^{-9} m/10^{-11} s = 100 m/s. For the conventional spin diffusion, the spin memory length is $l_s = \sqrt{D \cdot \tau_s}$, where $D = v_F^2 \tau / 3$ is the diffusion coefficient, τ_s is the Elliott-Yafet spin-relaxation time, τ is the charge transport relaxation time, and v_F is the Fermi velocity. For the purpose of order-of-magnitude estimation we define the spin-diffusion velocity v_s as $v_s = l_s / \tau_s = \sqrt{D/\tau_s}$, from which $v_s \approx 0.58 v_F \sqrt{\tau/\tau_s}$. Modern band-structure calculations [44,45] show that more than 95% of the electron density of states at Fermi energy comes from the itinerant 4*d*-electrons. The 3*d*-electrons Fermi velocity in iron-group ferromagnetic metals was a subject of interest in magnetic nanostructures [46-48] and had a value of about $3 \cdot 10^5$ m/s. Being stronger localized in the narrower 4*d*-bands [42] the conduction electrons must have lower velocity, say 10^5 m/s. Then, with the transport $\tau \sim 10^{-14}$ s and the electron-spin relaxation time $\tau_s \sim 10^{-9}$ s [49] we get $v_s \approx 1.8 \cdot 10^2$ m/s as an upper bound.

An order-of-magnitude matching of the obtained v_s value with the initial guess makes the 4*d*-electron spin-diffusion a plausible mechanism of the observed 10-25 ps demagnetization component in a mixed PM/FM state in the palladium-rich Pd-Fe alloys.

Conclusions

To conclude, based on the analysis of the experimental data on ultrafast optical and magneto-optical spectroscopy in comparison with the magnetometry data, we have identified the responses inherent in the magnetically inhomogeneous state of the $Pd_{1-x}Fe_x$ alloys epitaxial films. The vanishing of these components with decreasing temperature makes it possible to establish a lower limit for the concentration of the iron in the palladium and an operation temperature range that ensure the magnetically homogeneous ferromagnetic state of the films – one of the key requirements for their use as weak links in magnetic Josephson junctions and superconducting memory elements based on spin valves.

Acknowledgments

PAV, NSI, GAI, YIV, and YRV acknowledge the subsidy allocated to Kazan Federal University for the state assignment in the sphere of scientific activities No. FZSM-2020-0050. LRT thanks the support by a state assignment no. AAAA-A18-118030690040-8 to the Federal Research Center “Kazan Scientific Center of the Russian Academy of Sciences”.

References

1. Ryazanov, V.V.; Bol’ginov, V.V.; Sobanin, S.D.; Vernik, I.V.; Tolpygo, S.K.; Kadin, A.M.; Mukhanov, O.A. Magnetic Josephson junction technology for digital and memory applications. *Phys. Procedia* **2012**, *36*, 35–41. doi: 10.1016/j.phpro.2012.06.126
2. Tolpygo, S.K. Superconductor digital electronics: Scalability and energy efficiency issues. *Low Temp. Phys.* **2016**, *42*, 361-379. doi: 10.1063/1.4948618
3. Soloviev, I.I.; Klenov, N.V.; Bakurskiy, S.V.; Kupriyanov, M.Yu.; Gudkov, A.L.; Sidorenko, A.S. Beyond Moore’s technologies: operation principles of a superconductor alternative. *Beilstein J. Nanotechnol.* **2017**, *8*, 2689–2710. doi: 10.3762/bjnano.8.269
4. Braginski, A.I. Superconductor electronics: status and outlook. *J. Supercond. Novel Magn.* **2019**, *32*, 23–44. doi: 10.1007/s10948-018-4884-4
5. Schneider, M.L.; Donnelly, C.A.; Russek, S.E.; Baek, B.; Pufall, M.R.; Hopkins, P.F.; Dresselhaus, P.D.; Benz, S.P.; Rippard, W.H. Ultralow power artificial synapses using

nanotextured magnetic Josephson junctions, *Sci. Adv*. **2018**, *4*, e1701329. doi: 10.1126/sciadv.1701329

6. Mukhanov, O.A.; Semenov, V.K.; Likharev, K.K. Ultimate performance of RSFQ logic circuits. *IEEE Trans. Magn*. **1987**, *23*, 759–762. doi: 10.1109/TMAG.1987.1064951

7. Likharev, K.K. Superconductor digital electronics. *Physica C* **2012**, *482*, 6–18. doi: 10.1016/j.physc.2012.05.016

8. Mukhanov, O.A. Energy-efficient single flux quantum technology. *IEEE Trans. Appl. Supercond*. **2011**, *21*, 760-769. doi: 10.1109/TASC.2010.2096792

9. Herr, Q.P.; Herr, A.Y.; Oberg, O.T.; Ioannidis, A.G. Ultra-low-power superconductor logic. *J. Appl. Phys.* **2011**, *109*, 103903. doi: 10.1063/1.3585849

10. Holmes, D.S.; Ripple, A.L.; Manheimer M.A. Energy-efficient superconducting computing – power budgets and requirements. *IEEE Trans. Appl. Supercond*. **2013**, *23* 1701610. doi: 10.1109/TASC.2013.2244634

11. Volkmann, M.H.; Sahu, A.; Fourie, C.J.; Mukhanov O.A. Implementation of energy efficient single flux quantum digital circuits with sub-aJ/bit operation. *Supercond. Sci. Technol.* **2013**, *26*, 015002(16). doi:10.1088/0953-2048/26/1/015002

12. Bakurskiy, S.V.; Klenov, N.V.; Soloviev, I.I.; Bol'ginov, V.V.; Ryazanov, V.V.; Vernik, I.V.; Mukhanov, O.A.; Kupriyanov, M.Yu.; Golubov, A.A. Theoretical model of superconducting spintronic SIsFS devices. *Appl. Phys. Lett.* **2013**, *102*, 192603(4) doi: 10.1063/1.4805032

13. Vernik, I.V.; Bol'ginov, V.V.; Bakurskiy, S.V.; Golubov, A.A.; Kupriyanov, M.Yu.; Ryazanov, V.V.; Mukhanov, O.A. Magnetic Josephson junctions with superconducting interlayer for cryogenic memory, *IEEE Trans. Appl. Supercond*. **2013**, *23*, 1701208. doi: 10.1109/TASC.2012.2233270

14. Katam, N.K.; Mukhanov, O.A.; Pedram, M. Superconducting magnetic field programmable gate array. *IEEE Trans. Appl. Supercond.* **2018**, *28*, 1300212. doi: 10.1109/TASC.2018.2797262

15. Shafraniuk, S.E.; Nevirkovets, I.P.; Mukhanov, O.A. Modeling computer memory based on ferromagnetic/superconductor multilayers, *Phys. Rev. Appl.* **2019**, *11*, 064018. doi: 10.1103/PhysRevApplied.11.064018

16. Yamanashi, Y.; Nakaishi, S.; Yoshikawa, N. Simulation of the margins in single flux quantum circuits containing π-shifted Josephson junctions. *IEEE Trans. Appl. Supercond.* **2019**, *29*, 1301805. doi: 10.1109/TASC.2019.2904700

17. Ortlepp, T.; Ariando; Mielke, O.; Verwijs, V.C.M.; Foo, K.F.K.; Andreski, A.; Rogalla, H.; Uhlmann, F.H.; Hilgenkamp, H. RSFQ circuitry using intrinsic π-phase shifts. *IEEE Trans. Appl. Supercond.* **2007**, *17*, 659–663. doi: 10.1109/TASC.2007.898635

18. Khabipov, M.I.; Balashov, D.V.; Maibaum, F.; Zorin, A.B.; Oboznov, V.A.; Bolginov, V.V.; Rossolenko, A.N.; Ryazanov, V.V. A single flux quantum circuit with a ferromagnet-based Josephson π-junction. *Supercond. Sci. Technol.* **2010**, *23*, 045032. doi: 10.1088/0953-2048/23/4/045032

19. Feofanov, A.K.; Oboznov, V.A.; Bolginov, V.V.; Lisenfeld, J.; Poletto, S.; Ryazanov, V.V.; Rossolenko, A.N.; Khabipov, M.; Balashov, D.; Zorin, A.B.; Dmitriev, P.N.; Koshelets, V.P.; Ustinov, A.V. Implementation of superconductor/ferromagnet/superconductor π-shifters in superconducting digital and quantum circuits. *Nature Phys.* **2010**, *6*, 593–597. doi: 10.1038/NPHYS1700

20. Nevirkovets, I.P.; Chernyashevskyy, O.; Prokopenko, G.V.; Mukhanov, O.A. Superconducting-ferromagnetic transistor, *IEEE Trans. Appl. Supercond.* **2014**, *24*, 1800506(6). doi: 10.1109/TASC.2014.2318317

21. Yamanashi, Y.; Nakaishi, S.; Sugiyama, A.; Takeuchi, N.; Yoshikawa, N. Design methodology of single-flux-quantum flip-flops composed of both 0- and π-shifted Josephson junctions. *Supercond. Sci. Technol.* **2018**, *31*, 105003. doi: 10.1088/1361-6668/aad78d

22. Larkin,T.I.; Bol'ginov, V.V.; Stolyarov, V.S.; Ryazanov, V.V.; Vernik, I.V.; Tolpygo, S.K.; Mukhanov, O.A. Ferromagnetic Josephson switching device with high characteristic voltage *Appl. Phys. Lett*. **2012**, *100*, 222601. doi: 10.1063/1.4723576

23. Baek, B.; Rippard, W.H.; Benz, S.P.; Russek, S.E.; Dresselhaus, P.D. Spin-transfer torque switching in nanopillar superconducting-magnetic hybrid Josephson junctions. *Nature Commun.* **2014**, *5*, 3888. doi: 10.1038/ncomms4888

24. Gingrich, E.C.; Niedzielski, B.M.; Glick, J.A.; Wang, Y.; Miller, D.L.; Loloee, R.; Pratt Jr, W.P.; Birge, N.O. Controllable 0–π Josephson junctions containing a ferromagnetic spin valve. *Nature Phys.* **2016**, *12*, 564–567. doi: 10.1038/nphys3681

25. Nevirkovets, I.P.; Shafraniuk, S.E.; Mukhanov, O.A. Multiterminal superconducting-ferromagnetic device with magnetically tunable supercurrent for memory application. *IEEE Trans. Appl. Supercond.* **2018**, *28*, 1800904. doi: 10.1109/TASC.2018.2836938

26. Dayton, I.M.; Sage, T.; Gingrich, E.C.; Loving, M.G.; Ambrose, T.F.; Siwak, N.P.; Keebaugh, N.P.; Kirby, C.; Miller, D.L.; Herr, A.Y.; Herr, Q.P.; Naaman, O. Experimental demonstration of a Josephson magnetic memory cell with a programmable π-junction. *IEEE Magnet. Lett.* **2018**, *9*, 3301905. doi: 10.1109/LMAG.2018.2801820

27. Esmaeili, A.; Yanilkin, I.V.; Gumarov, A.I.; Vakhitov, I.R.; Gabbasov, B.F.; Kiiamov, A.G.; Rogov, A.M.; Osin, Yu.N.; Denisov, A.E.; Yusupov, R.V.; Tagirov, L.R. Epitaxial growth of $Pd_{1-x}Fe_x$ films on MgO single-crystal substrate. *Thin Solid Films* **2019**, *669*, 338–344. doi: 10.1016/j.tsf.2018.11.015

28. Esmaeili, A.; Yanilkin, I.V.; Gumarov, A.I.; Vakhitov, I.R.; Gabbasov, B.F.; Yusupov, R.V.; Tatarsky, D.A.; Tagirov, L.R. Epitaxial thin-film $Pd_{1-x}Fe_x$ alloy – a tunable ferromagnet for superconducting spintronics. *Sci. China Mater. (Springer)* **2021**, *63*, 1–10. doi: 10.1007/s40843-020-1479-0

29. Niedzielski, B.M.; Diesch, S.G.; Gingrich, E.C.; Wang, Y.; Loloee, R.; Pratt. Jr.W.P.; Birge, N.O. Use of Pd–Fe and Ni–Fe–Nb as soft magnetic layers in ferromagnetic Josephson junctions for nonvolatile cryogenic memory. *IEEE Trans. Appl. Supercond*. **2014**, *24*, 1800307(7). doi: 10.1109/tasc.2014.2311442

30. Glick, J.A., Loloee, R.; Pratt. Jr.W.P.; Birge, N.O. Critical current oscillations of Josephson junctions containing PdFe nanomagnets. *IEEE Trans. Appl. Supercond.* **2017**, *27*, 1800205(5). doi: 10.1109/TASC.2016.2630024

31. Uspenskaya, L.S.; Khlyustikov, I.N. Anomalous magnetic relaxation in thin $Pd_{0.99}Fe_{0.01}$ films. *J. Exp. Theor. Phys*. **2017**, *125*, 875-878. doi: 10.1134/S1063776117100090.

32. Nieuwenhuys, G.J. Magnetic behaviour of cobalt, iron and manganese dissolved in palladium. *Adv. Phys*. **1975**, *24*, 515-591. doi: 10.1080/00018737500101461

33. Korenblit, I.Ya.; Shender, E.F. Ferromagnetism of disordered systems. *Sov Phys – Uspekhi* **1978**, *21*. 832-851. doi: 10.1070/PU1978v021n10ABEH005686

34. Ewerlin, M.; Pfau, B.; Günther, C.M.; Schaffert, S.; Eisebitt, S.; Abrudan, R.; Zabel, H. Exploration of magnetic fluctuations in PdFe films. *Journ. Phys.: Cond. Matter* **2013**, *25*: 266001. doi: 10.1088/0953-8984/25/26/266001

35. Petrov, A.V.; Yusupov, R.V.; Nikitin, S.I.; Gumarov, A.I.; Yanilkin, I.V.; Kiiamov, A.G.; Tagirov, L.R. Femtosecond optical and magneto-optical spectroscopy study of magnetic and electronic inhomogeneities in a $Pd_{0.94}Fe_{0.06}$ thin film. *JETP Letters* **2019**, *109*, 266–269. doi: 10.1134/S0021364019150104

36. Knorren, R.; Bouzerar, G.; Bennemann, K.H. Theory for the dynamics of excited electrons in noble and transition metals, J. Phys.: Condens. Matter **2002**, *14*, R739. stacks.iop.org/JPhysCM/14/R739.

37. Koopmans, B.; Malinowski, G.; Dalla Longa, F.; Steiauf, D.; Fähnle, M.; Roth, T.; Cinchetti, M.; Aeschlimann, M. Explaining the paradoxical diversity of ultrafast laser-induced demagnetization. Nature materials **2010**, *9*, 259-265. doi: 10.1038/NMAT2593

38. Melnikov, A.; Razdolski, I.; Wehling, T.O.; Papaioannou, E. Th.; Roddatis, V.; Fumagalli, P.; Aktsipetrov, O.; Lichtenstein, A.I.; Bovensiepen, U. Ultrafast Transport of Laser-Excited Spin-Polarized Carriers in Au/Fe/MgO (001), *Phys. Rev. Lett.* **2011**, *107*, 076601. doi: 10.1103/PhysRevLett.107.076601

39. Fähnle, M.; Illg, C. Electron theory of fast and ultrafast dissipative magnetization dynamics, J. Phys.: Condens. Matter **2011**, *23*, 493201. doi:10.1088/0953-8984/23/49/493201

40. Kirilyuk, A.; Kimel,; A.V.; Rasing, Th. Laser-induced magnetization dynamics and reversal in ferrimagnetic alloys, Rep. Prog. Phys. **2013**, *76*, 026501. doi:10.1088/0034-4885/76/2/026501.

41. Wang Ch,; Liu, Y. Ultrafast optical manipulation of magnetic order in ferromagnetic materials. Nano Convergence **2020**, *7*, 35. doi: 10.1186/s40580-020-00246-3.

42. Alekhin, A.; Razdolski, I.; Berritta, M.; Bürstel, D.; Temnov, V.; Diesing, D.; Bovensiepen, U.; Woltersdorf, G.; Oppeneer, P.M.; Melnikov, A. Magneto-optical properties of Au upon the injection of hot spin-polarized electrons across Fe/Au (001) interfaces. *Journ. Phys.: Cond. Matter* **2019**, *31*, 124002. doi: 10.1088/1361-648X/aafd06

43. Wieczorek, J.; Eschenlohr, A.; Weidtmann, B.; Rösner, M.; Bergeard, N.; Tarasevitch, A.; Wehling, T.O.; Bovensiepen, U. Separation of ultrafast spin currents and spin-flip scattering in Co/Cu (001) driven by femtosecond laser excitation employing the complex magneto-optical Kerr effect. *Physical Review B* **2015**, *92*, 174410. doi: 10.1103/PhysRevB.92.174410

44. Östlin, A.; Appelt, W.H.; Di Marco, I.; Sun, W.; Radonjić, M.; Sekania, M.; Vitos, L.; Tjernberg, O.; Chioncel, L. Electronic structure of palladium in the presence of many-body effects, *Physical Review B* **2016**, *93*, 155152. doi: 10.1103/PhysRevB.93.155152

45. Setayandeh, S.S.; Webb, C.J.; Gray, E. Electron and phonon band structures of palladium and palladium hydride: A review, *Progress in Solid State Chemistry* **2020**, *60*, 100285. doi: 10.1016/j.progsolidstchem.2020.100285

46. Petrovykh, D.Y.; Altmann, K.N.; Höchst, H.; Laubscher, M.; Maat, S.; Mankey, G.J.; Himpsel, F.J. Spin-dependent band structure, Fermi surface, and carrier lifetime of permalloy, *Applied Physics Letters* **1988**, *73*, 3459–3461. doi: 10.1063/1.122796

47. Himpsel, F.J.; Altmann, K.N.; Mankey, G.J.; Ortega, J.E.; Petrovykh, D.Y. Electronic states in magnetic nanostructures, *Journal of Magnetism and Magnetic Materials* **1999**, *200*, 456–469. doi: 10.1016/S0304-8853(99)00349-2

48. Altmann, K.N.; Gilman, N.; Hayoz, J.; Willis, R.F.; Himpsel, F.J. Effect of Magnetic Doping on the Electronic States of Ni, *Physical Review Letters* **2001**, *87*, 137201. doi: 10.1103/PhysRevLett.87.137201.

49. Koopmans, B.; Ruigrok, J.J.M.; Dalla Longa, F.; de Jonge, W.J.M. Unifying ultrafast magnetization dynamics. *Phys. Rev. Lett.* **2005**, *95*, 267207. doi: 10.1103/PhysRevLett.95.267207